Austin Chemical Engineering

Open Access

Austin Publishing Group

Review Article

Effect of Ti doping on the Structural, Magnetic and Magnetocaloric Properties of the Sample $Pr_{0.9}Sr_{0.1}Mn_{0.95}Ti_{0.05}O_3$

Rahal O[1]; Ellouze M[1*]; Ates S[2]; Hlil EK[3]

[1]Sfax University, Faculty of Sciences of Sfax, LM2EM, B.P. 1171, 3000, Sfax, Tunisia

[2]Sivas Cumhuriyet University, Engineering Faculty, Department of Chemical Engineering, 58140, Sivas, Türkiye

[3]University Grenoble Alpes, CNRS, Grenoble INP, Institute Néel, 38000 Grenoble, France

***Corresponding author: Ellouze M**

Sfax University, Faculty of Sciences of Sfax, LM2EM, B.P. 1171, 3000, Sfax, Tunisia.

Tel: +216 98 414 707

Email: Mohamed.ellouze@fss.rnu.tn

Received: April 25, 2023

Accepted: June 03, 2023

Published: June 10, 2023

Abstract

In this paper, was investigated the impact of Ti substitution at the Mn-site in manganite on the structural, magnetic, and magnetocaloric properties of the sample $Pr_{0.9}Sr_{0.1}Mn_{0.95}Ti_{0.05}O_3$ prepared by solid-solid reaction. X-ray diffraction was used for the structural studies and the Rietveld refinement shows that the compound is crystallized in a Pnma space group. Williamson-Hall (W-H) analysis was used to determine the crystallites' sizes. Scanning Electron Microscopy (SEM) was used to determine the surface morphology of the compound and the grain size which was determined using ImageJ software. The magnetic properties are treated using the BS1 magnetometer in which we obtained a phase transition from a ferromagnetic FM state to a paramagnetic PM state around the Curie temperature T_C which simply decreases from the mother, indicating the weakness of the double exchange interaction. The sample's aptitude to be used in magnetic refrigeration demonstrated by the value of maximum entropy $|\Delta S_m^{max}|$ is 3.7812 J $Kg^{-1}.K^{-1}$, which corresponds to the best Relative Cooling Power (RCP) 207.1227 J Kg^{-1} at 5T magnetic field applied compared to Gadolinium (Gd). The Modified Arrott Plot (MAP) is used to understand the FM-PM transition's nature, and it is through this curve that critical exponent β, γ and curie temperature were determined using the MAP and Fisher methods. The critical coefficient values for β, γ and T_C determined by different techniques, are correspondingly similar to the values of the Mean-Field model's.

Keywords: Manganite; Magnetocaloric effect; Arrott plots; Critical behavior; Landau theory

Introduction

Praseodymium manganite $Pr_{1-x}A_x MnO_3$ where A is an alkaline earth ion (such as Ca, Ba, or Sr) is a very important element in the large family of manganites because of its fundamental physical properties and its exploitation in practical uses. Therefore, much research is being done today on this manganite, particularly since the discovery of the phenomena known as Colossal Magnetoresistance (CMR) and Magnetocaloric Effect (MCE) [1,2]. Because these magnetic materials can be utilized for Magnetic Refrigeration (MR), the widespread use of manganite makes it an excellent cooling solution compared to the use of gas refrigeration technology in the future. Thus, it is possible to create a cleaner environment and reduce pollution by using Magnetic Refrigeration (MR) based on manganite [3]. The simplicity of preparation, low prices, and ability to create a novel material magnetic use in the use of magnetocaloric effect MCE in a wide temperature range which is based on the magnetic refrigeration are the benefits of these perovskite manganese oxides [4].

When a magnetic material is exposed to an applied magnetic field, its entropy changes. This change leads to a change in temperature and is the basis of the Magnetocaloric Effect (MCE) [5]. There exists a large magnetic entropy around the paramagnetic-ferromagnetic transition temperature (Tc). Wide range techniques could change the Curie temperature T_C has been observed in manganite regardless of the percentage, nature, and location of the dopant. The different elements could dope the manganese ion in manganite are It, Cr, Fe, etc. [6].

In the work we focused to study the effect of Ti doped substitution of Mn, on the structural, magnetic and magnetocaloric

Citation: Rahal O, Ellouze M, Ates S, Hlil EK. Effect of Ti doping on the Structural, Magnetic and Magnetocaloric Properties of the Sample $Pr_{0.9}Sr_{0.1}Mn_{0.95}Ti_{0.05}O_3$. Austin Chem Eng. 2023; 10(1): 1095.

properties of the compound $Pr_{0.9}Sr_{0.1}Mn_{0.95}Ti_{0.05}O_3$.

Experimental Details

To prepare compound $Pr_{0.9}Sr_{0.1}Mn_{0.95}Ti_{0.05}O_3$ by ceramic reaction (solid-solid), we used the following oxides as precursors Pr_6O_{11}, MnO_2, $SrCO_3$, TiO_2 which were weighed in the required stoichiometric proportions by the following reaction equation:

$$0.15\ Pr_6O_{11} + 0.1\ SrCO_3 + 0,\ 0.95\ MnO_2 + 0.05\ TiO_2 \rightarrow Pr_{0.9}Sr_{0.1}Mn_{0.95}Ti_{0.05}O_3 + CO_2$$

We first mixed the precursors together in an agate mortar. Subsequently, the mixture was calcined in for 72 hours at 1000°C followed by grinding. Then the powder was pressed and transformed into pellet 10mm in diameter and 1mm-2mm in thickness which finally was sintered after in air at 1200°C for 96h to obtain a homogeneous material. The sample was ground again and annealed at 1200°C.

To identify the structures and phases of the synthesized compounds, the X-Ray Diffraction (XRD) was used with a Siemens "D5000" diffractometer equipped with a probe (λ_{Cu}=1.5406 Å) and measured at a spacing of 0.026° in the angular range 20-80 degrees. The diffraction pattern obtained from XRD was analyzed using comprehensive Full proof software [7] based on Rietveld method [8]. The morphology of the surface of the sample were obtained using Scanning Electron Microscopy (SEM) (Tescan® Mira3 XMU, Czechia) instrument and the grain size was calculated using ImageJ software by adjusting the Gaussian function. The analysis of magnetism and magnetization depending on the temperature from 5K to 400K at a magnetic field up to 5T was made by the BS1 magnetometer which was also used for this study. The magnetic thermal analysis allowed to define the magnetocaloric effect under a magnetic field applied from 1T to 5T.

Results and Discussion

The Rietveld refinement of powder X-ray diffraction (Figure 1) was used to determine the structure of the sample. It has an orthorhombic structure with space group Pnma. There is no secondary phase was detected by the diffractogram measurements as shown in Figure 1, revealing that the sample is a single phase.

To determine the distortion of the synthesized sample, the Goldschmidt tolerance factor t of perovskite is used, which is given by the following expression:

$$t = \frac{r_A + r_O}{\sqrt{2}(r_B + r_O)} \qquad (1)$$

where r_A is an ionic radius of the cation occupying site A, r_B is an ionic radius of the cation occupying the B site, r_O is an ionic radius of oxygen. The value of ionic radius used is r_{Pr}^{3+}=1.179 Å, r_{Sr}^{2+}=1.31 Å, r_{Mn}^{3+}=0.645 Å, r_{Mn}^{4+}=0.53 Å, r_O^{2-}=1.405 Å, r_{Ti}^{4+}=0.605 Å [10].

Indeed, it was found the increasing value of Volume cell (V) with a 5% of Ti doping in parent compound, which is explained by increasing in lattice parameters and the rising of the ionic radius of Ti^{4+} (0.605 Å). The refined lattice parameters of the sample, the Goldschmidt [9] tolerance factor t and crystallite size D_{WH} is summarized in Table 1,

From the atomic occupation of the different elements as shown in Table 2, it could be representing the unit cell using the "Diamond" program (Figure 2) which we have determined the different distances Mn/Ti-O and angles O– M n/ Ti- O distances. (The sentence can be simplified). A change in the distance of the compound compared to the parent sample showed the octahedral irregularity of MnO_6 and thus less distortion of the structure when in manganite the Manganese (Mn) ion is doped by 5% of Titanium (Ti) ion.

The morphology and the crystal grains distribution of the $Pr_{0.9}Sr_{0.1}Mn_{0.95}Ti_{0.05}O_3$ compound are shown in Figure 3. The particle has an aspherical shape, and the average grain size determined with Image J software is 5.08µm. This is due to formation of many crystallites.

In addition, the crystallite size D_{WH} is calculated by the Williamson–Hall (W–H) method [11] given by:

$$\hat{a}\cos\grave{e} = K\lambda / D_{WH} + 4\varepsilon sin\theta \qquad (2)$$

where K: constant equal to 0.9, **λ: wavelength of the X radiation** (λ=1.5406 Å), θ: the diffraction angle of the peak, β: the full width at half maximum, ε: the effective strain.

The W-H curves are shown in Figure 4 and value of ε and D_{WH} are calculated the by linear fit summarized in Table 1. The value of the effective strain ε was estimated from the slope β cos θ vs. 4 sin θ plot (Figure 4) and D_{WH} was calculated from the intercept with vertical axes. Noted that the grain size is bigger than the D_{WH} estimated crystallite size of 28.24µm.

The magnetization curve versus temperature in the temperature M (T) from 5 K to 400 K under a magnetic field of 0.05 T (Figure 5) shows a phase transition from a ferromagnetic FM state to a paramagnetic PM state. This transition is characterized by the Curie temperature T_C determined at the minimum of the dM/dT curve versus temperature (Figure 5). The purity of $Pr_{0.9}Sr_{0.1}Mn_{0.95}Ti_{0.05}O_3$ has been approved by the continuity of FM-PM transition. Also, it was reported that a decrease of the Curie temperature T_C from 214.9 K to 95.11 K while doping the parent sample $Pr_{0.9}Sr_{0.1}MnO_3$ [12] with 5% Ti in Mn site, which is explained by a reduction of the double exchange interaction [13]. The decrease in the rate of Mn^{4+} carriers and their substitution by the nonmagnetic Ti^{4+} ion caused this weakening and breaking of Double Exchange (DE) interaction which was affected the undoing of the electronic conduction shift e_g between Mn^{4+} et Mn^{3+} and explained by the converting of the Mn^{3+}-O-Mn^{4+} chain to Mn^{3+}-O- Ti^{4+} that's diminished the ferromagnetic interactions.

To understand and know more the magnetic properties of the sample in the paramagnetic phase, the susceptibility the magnetic should be obey to the Weiss Curie law [14]:

$$\chi = \frac{C}{\text{Ť} - \text{ù}} \qquad (3)$$

Where C is the curie constant and θ_ω is a Curie-Weiss temperature.

Figure 6 showed the inverse of the magnetic susceptibility (1/χ) versus temperature at a magnetic field of 0.05 T, which can help to calculate the Curie constant C and Curie- Weiss temperature θ_ω. The values of C and θ_ω are estimated by the slope and the intercept with the temperature axis of the linear fit in paramagnetic phase, respectively.

From the value of the Curie constant C obtained, the experimental effective moment can be calculated according to the following formula [15]:

$$(\mu_{eff}^{ex})^2 = \frac{3k_B}{N_A\mu_B^2}C \qquad (4)$$

Where: N_A=6.023 10^{23} mol^{-1} is the Avogadro number,

μ_B=9.274 10^{-24} Am^2 is the Bohr magneton, and k_B=1.38 10^{-23} is the Boltzmann constant

In contrast, the theoretical effective moment of the compound is calculated from the carrier effective moments using the following formula:

$$\mu_{eff}^{th} = \sqrt{0.9 * \mu_{eff}^2(Mn^{3+}) + 0.05 * \mu_{eff}^2(Mn^{4+}) + 0.9 * \mu_{eff}^2(Pr^{3+})} \quad (6)$$

$\mu_{eff}(Mn^{4+})$= 3.87μ_B, $\mu_{eff}(Mn^{3+})$= 4.9μ_B, $\mu_{eff}(Pr^{3+})$= 3.58 μ_B [15]

The results summarized in Table 3 indicates that the values of the experimental and theoretical effective moment of the sample are different. This difference can be explained by the presence of clusters FM in the state PM as described by Zener model [16].

Table 1: Lattice parameters, unit cell volume, Goldschmidt tolerance factor t, D_{WH} and strain ε of our sample $Pr_{0.9}Sr_{0.1}Mn_{0.95}Ti_{0.05}O_3$ (the numbers in subscript represent the error).

	$Pr_{0.9}Sr_{0.1}Mn_{0.95}Ti_{0.05}O_3$	$Pr_{0.9}Sr_{0.1}MnO_3$ [12]
a (Å)	5.4935_6	5.49165
b (Å)	7.7889_3	7.78377
c (Å)	5.5498_1	5.54722
V (Å3)	237.47	237.11
Good Fit x^2	2.19	2.31
Goldschmidt tolerance factor	0.899	0.89
D_{WH} (μm)	28.24	-
ε	0.00279	-

Table 2: Refined positions, distances Mn-O and angles Mn-O-Mn of $Pr_{0.9}Sr_{0.1}Mn_{0.95}Ti_{0.05}O_3$ compared with $Pr_{0.9}Sr_{0.1}MnO_3$ [12] (the numbers in subscript represent the error).

Samples	$Pr_{0.9}Sr_{0.1}Mn_{0.95}Ti_{0.05}O_3$	$Pr_{0.9}Sr_{0.1}MnO_3$ [12]
Pr/Sr		
x	-0.0378_5	-0.0398_2
y	0.25	0.25
z	0.0083_1	0.0079_3
Mn/Ti		
x	0	0
y	0	0
z	0.5	0.5
O_1		
x	0.5244_2	0.5132_4
y	0.25	0.25
z	-0.0684_2	-0.0804_7
O2		
x	0.2925_8	0.2891_6
y	-0.0282_7	-0.0341_1
z	0.7983_4	0.7113_2
Distances		
Mn-O_1 (Å)	1.988	1.998
Mn-O_{21} (Å)	2.138	1.991
Mn-O_{22} (Å)	1.613	1.994

Table 3: The values of the experimental and theoretical effective moment of the sample $Pr_{0.9}Sr_{0.1}Mn_{0.95}Ti_{0.05}O_3$.

C (K.emu/mol Oe)	$\theta_\omega(K)$	$\mu_{eff}^{ex}(\mu_B)$	$\mu_{eff}^{th}(\mu_B)$
		$\mu_{eff}^{ex}(\mu_B)$	$\mu_{eff}^{th}(\mu_B)$
11.77	103.59	9.70	5.82

Table 4: Maximum entropy change $|\Delta S^{max}_M|$, RCP, δT_{FWHM} and $|\Delta C^{max}_p|$ of the sample $Pr_{0.9}Sr_{0.1}Mn_{0.95}Ti_{0.05}O_3$

Sample	$\mu_0 H$ (T)	$-\Delta S^{max}_M$ ($J\,Kg^{-1}K^{-1}$)	δT_{FWHM} (K)	RCP ($J\,Kg^{-1}$)	$\lvert\Delta C^{max}_p\rvert$ ($J\,Kg^{-1}K^{-1}$)
$Pr_{0.9}Sr_{0.1}Mn_{0.95}Ti_{0.05}O_3$	1	0.970	43.012	41.752	3.1615
	2	1.791	51.285	91.851	4.8145
	3	2.516	56.049	141.018	6.0169
	4	3.172	57.384	182.044	6.684
	5	3.781	54.777	207.123	7.058
Gd [1]	5	9.5	-	410	-

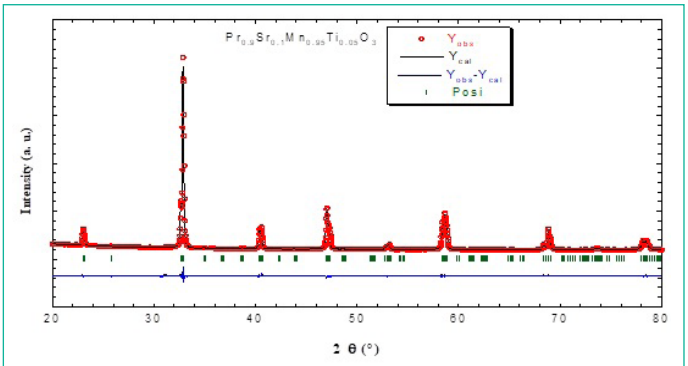

Figure 1: Observed and calculated X-ray diffraction data and Rietveld refinement for $Pr_{0.9}Sr_{0.1}Mn_{0.95}Ti_{0.05}O_3$. Vertical bars are the Bragg reflections for the space group Pnma. The difference pattern between the observed data and fits is shown at the bottom.

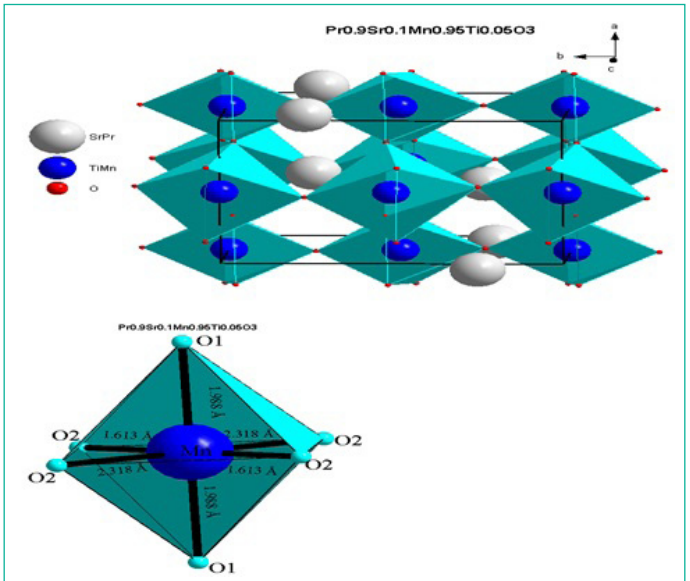

Figure 2: Crystallographic structure of $Pr_{0.9}Sr_{0.1}Mn_{0.95}Ti_{0.05}O_3$ sample.

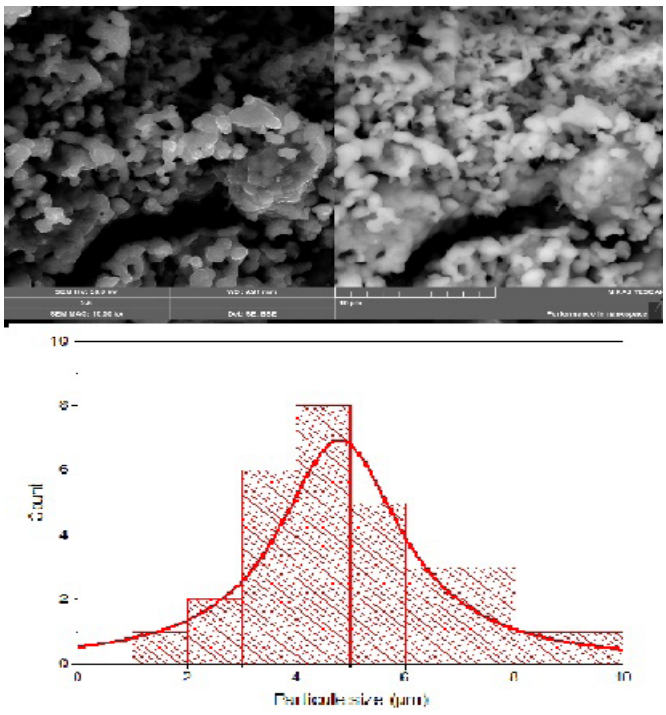

Figure 3: The Williamson–Hall analysis plots of $Pr_{0.9}Sr_{0.1}Mn_{0.95}Ti_{0.05}O_3$ sample.

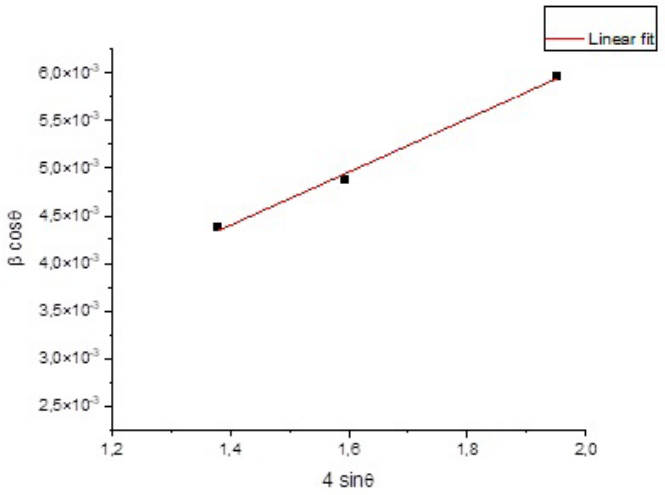

Figure 4: SEM picture of the compound $Pr_{0.9}Sr_{0.1}Mn_{0.95}Ti_{0.05}O_3$.

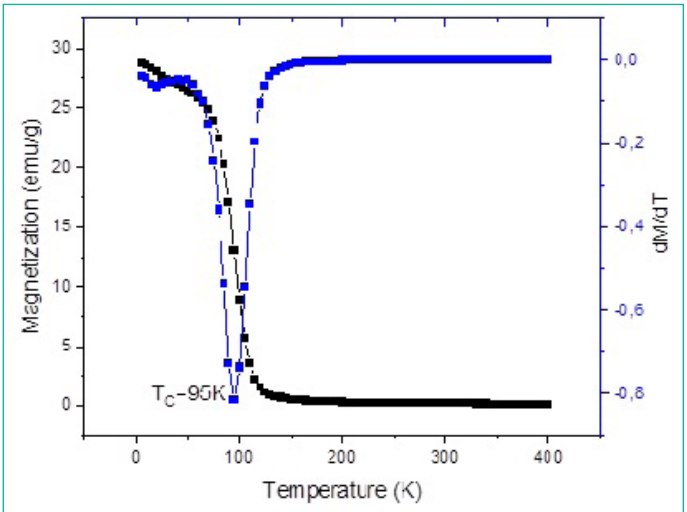

Figure 5: The temperature dependence of magnetization and dM/dT curves performed under applied magnetic field 0.05 T.

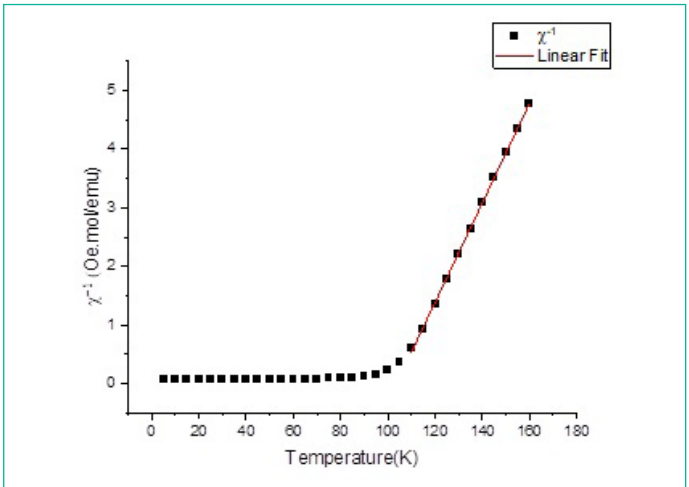

Figure 6: Variation of the inverse of the susceptibility as a function of the temperature of $Pr_{0.9}Sr_{0.1}Mn_{0.95}Ti_{0.05}O_3$.

Table 5: Critical exponents of $Pr_{0.9}Sr_{0.1}Mn_{0.95}Ti_{0.05}O_3$ with those corresponding to the various critical.

Technique	TC (K)	β (K)	γ	Reference
Mean-Field model	-	0.5	1	[24]
3D-Heisenberg model	-	0.365	1.336	[24]
3D-Ising model	-	0.325	1.24	[24]
Tricritical mean-Field model	-	0.25	1	[24]
MAP	93.47	0.47	1.36	This work
KF	94.23	0.5	1.41	This work

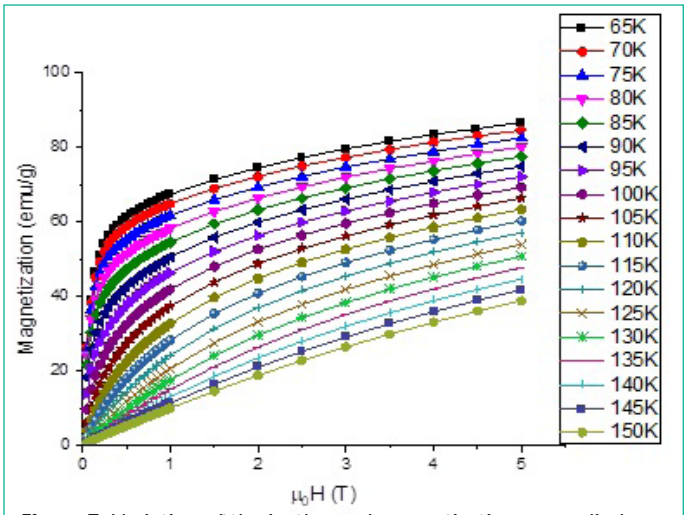

Figure 7: Variation of the isothermal magnetization v.s applied magnetic field at different temperatures for the compound $Pr_{0.9}Sr_{0.1}Mn_{0.95}Ti_{0.05}O_3$.

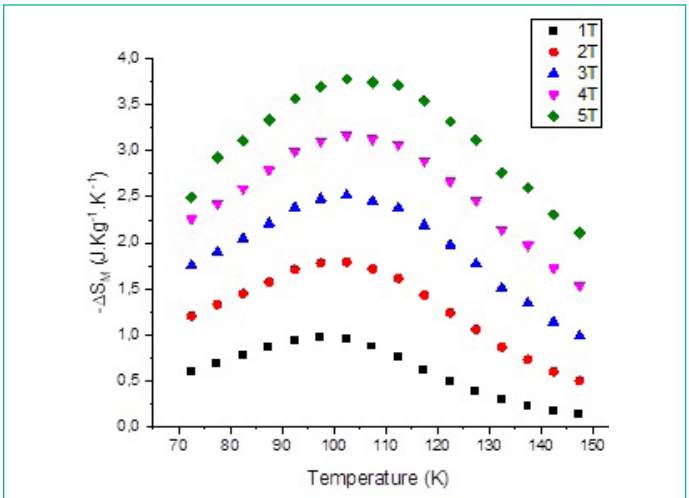

Figure 8: Dependence magnetic entropy versus the temperature of our sample $Pr_{0.9}Sr_{0.1}Mn_{0.95}Ti_{0.05}O_3$.

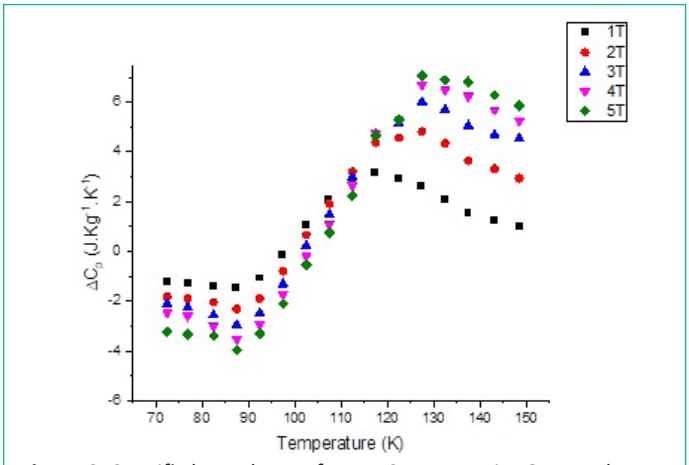

Figure 9: Specific heat change for $Pr_{0.9}Sr_{0.1}Mn_{0.95}Ti_{0.05}O_3$ sample under different applied magnetic fields.

Magnetocaloric Effect

The magnetization as a function of temperature and magnetic applied field from 1T to 5T of our compound $Pr_{0.9}Sr_{0.1}Mn_{0.95}Ti_{0.05}O_3$ was plotted in Figure 7. We notice that the magnetization is raised at low temperatures when $T< T_C$ and $\mu_0 H < 0.5T$, which reveals the coexistence of ferromagnetic order brought on by thermal agitation. For $T>T_C$ the magnetization is oriented toward linearity, confirming the paramagnetic state of the sample.

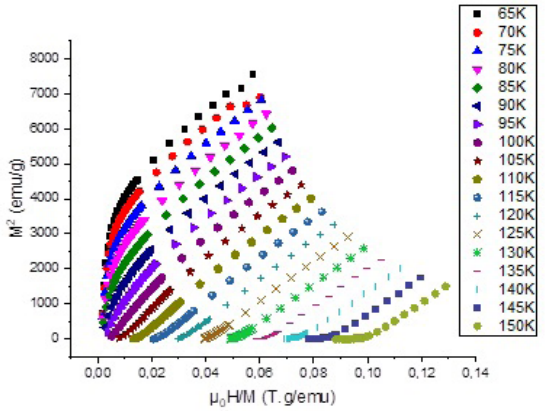

Figure 10: Arrott plots of $Pr_{0.9}Sr_{0.1}Mn_{0.95}Ti_{0.05}O_3$.

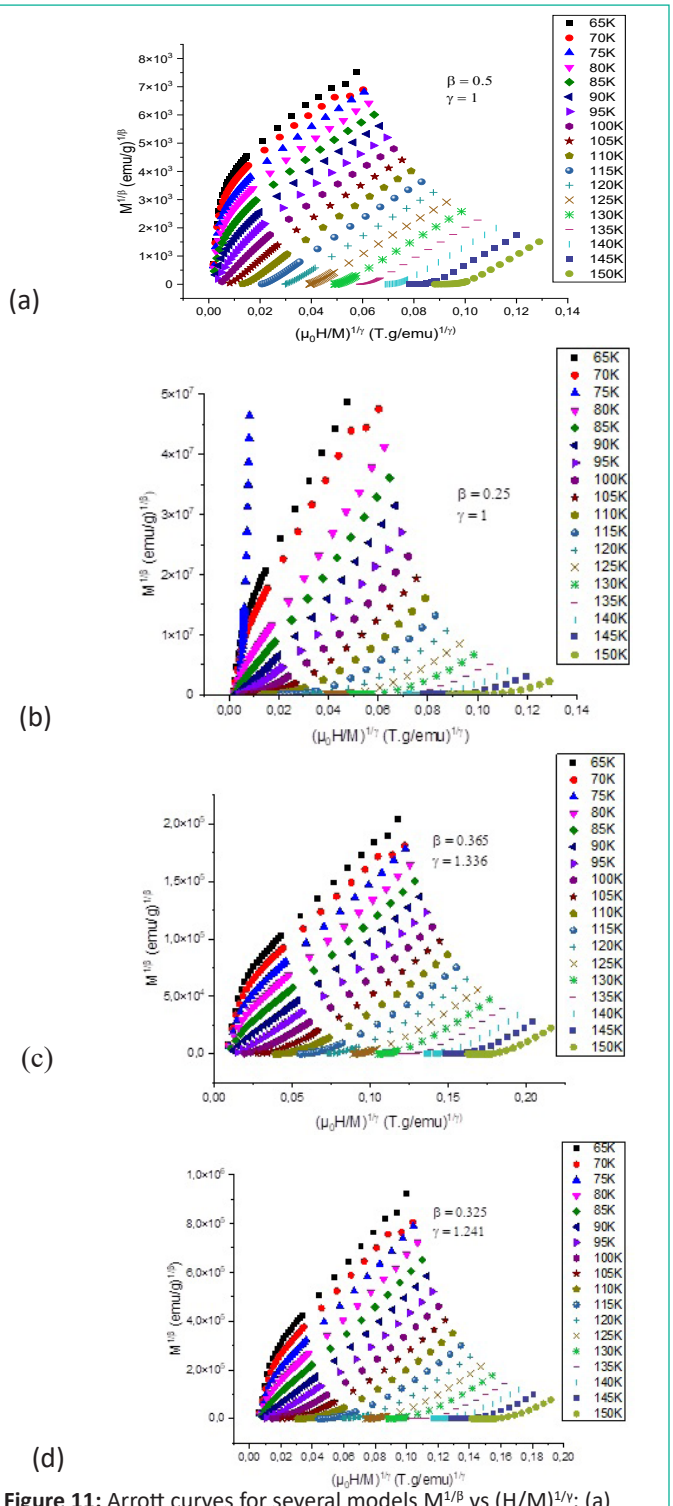

Figure 11: Arrott curves for several models $M^{1/\beta}$ vs $(H/M)^{1/\gamma}$: (a) Mean-Field model, (b) Tricritical mean-Field model, (c) 3D-Heisenberg model and (d) 3D-Ising model .

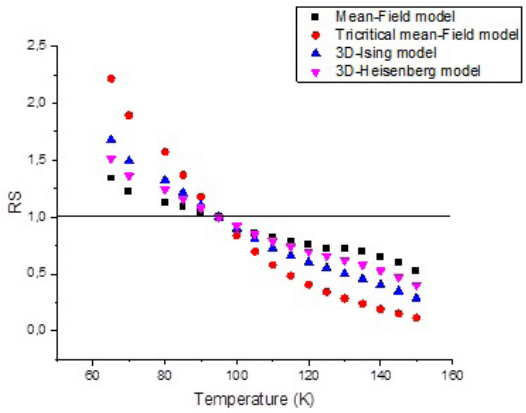

Figure 12: Relative slope RS versus temperature.

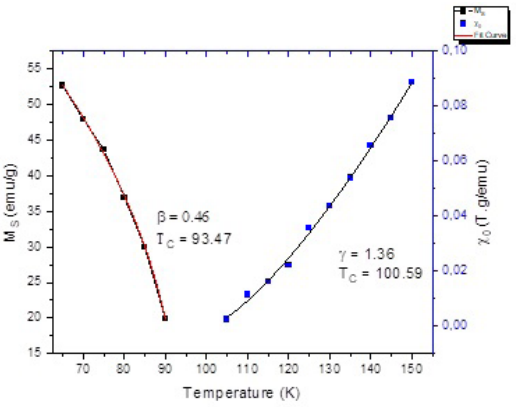

Figure 13: The spontaneous magnetization M_s and inverse susceptibility χ_0^{-1} vs. temperature for the compound $Pr_{0.9}Sr_{0.1}Mn_{0.95}Ti_{0.05}O_3$.

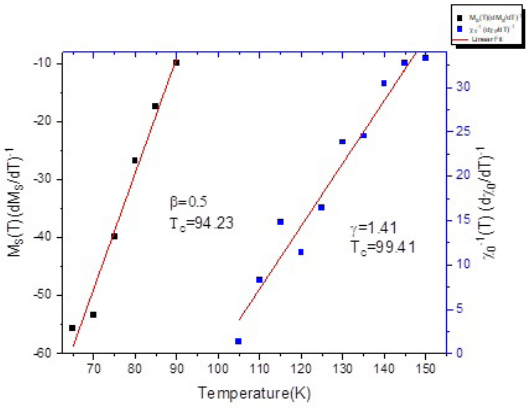

Figure 14: Kouvel –Fisher plots for the spontaneous magnetization M_s and inverse susceptibility χ_0^{-1} vs. temperature for the compound $Pr_{0.9}Sr_{0.1}Mn_{0.95}Ti_{0.05}O_3$.

The study of Magnetocaloric Effect (MCE) of the sample is based on the investigation of the entropy fluctuation as a function of temperature and magnetic field from 1T to 5T.

The calculation of the change of the magnetic entropy (ΔS_M) is achieved from Maxwell's relation [17] by analyzing the isothermal magnetization data shown in Figure 7.

$$\Delta S_M(T, H_{max}) = S_M(T, H_{max}) - S_M(T, 0) = \int_0^{H_{max}} \left(\frac{\partial M}{\partial T}\right) dH(T, H_{max}) \quad (5)$$

The discretization into small intervals of temperature and magnetic field allowed us to calculate the evolution of the entropy (ΔS_M) using the following relation [18]:

$$|\Delta S_M| = \sum_i \frac{M_i - M_{i+1}}{T_{i+1} - T_i} \Delta H_i \quad (6)$$

The Figure 8 represents the variation of the magnetic en-

tropy ($-\Delta S_M$) as a function of temperature and magnetic field. A maximum of the entropy ($-\Delta S_M$) has been recorded at a temperature near the Curie temperature for all applied magnetic field. We also saw that the magnetic field had an impact on the maximum magnetic entropy value, which can be explained by arrangement of the spin [19]. For instance, when the magnetic application changes from 1 to 5T, the value of $-\Delta S_M$ of sample $Pr_{0.9}Sr_{0.1}Mn_{0.95}Ti_{0.05}O_3$ increases from 0.97 J/Kg K to 3.78 J/Kg K.

The Magnetocaloric Effect (MCE) is an important factor for the Relative Cooling Power (RCP) that allows comparing the magnetic materials utilized for magnetic refrigeration. The relationship between factor RCP and the change of entropy $-\Delta S_M$ is given by the following equation [20]:

$$RCP = -\Delta S_M^{\max} \times \delta T_{FWHM} \qquad (7)$$

where δT_{FWHM} is the Full-Width at half maximum of the peak of $-\Delta S_M$ as a function of temperature and $-\Delta S_M^{max}$ is its maximum value, which occurs near T_C.

The obtained values of RCP, $-\Delta S_M{}^{max}$ and δT_{FWHM} are summarized in Table 4. The value of RCP rises from 41.75 J/K to 207.12 J/K for 1 T to 5 T, respectively. These results show that the sample can be used in the field of magnetic refrigeration compared to Gd.

From the measurement of the magnetic entropy, the specific heat ΔC_p for various applied magnetic field intensities is determined by using the following equation [21].

$$\Delta C_p(T,H) = C_p(T,H) - C_p(T,0) = T\left[\frac{\partial(\Delta S_M(T,H)}{\partial T}\right] \qquad (8)$$

Figure 9 illustrates the changes in specific heat ΔC_p with temperature and with an applied magnetic field from 1 to 5T. According to Figure 9, the change of ΔC_p from negative value to positive value with the Curie temperature indicates the phase transition. All obtained values of the maximum amount of the change in specific heat $\Delta C_p{}^{max}$ is summarized in Table 4.

Critical Behavior

The Arrott plots of the compound $Pr_{0.9}Sr_{0.1}Mn_{0.95}Ti_{0.05}O_3$ are shown in Figure 10. The analysis of the Arrott curve M^2 as a function of ($\mu_0 H/M$) reveals the nature of the transition. According to the criterion proposed by Banerjee et al. [22], the slope of the resulting curves can indicate whether the magnetic transition is of the first order (negative slope) or the second order (positive slope).

The curves clearly show a positive slope in the whole temperature range studied revealing that the ferromagnetic-paramagnetic transition is of the second order.

Arrott curve in Figure 10 was examined to analysis the magnetic characteristics. Arrott curve modification (MAP) was used by the basic equation [23]:

$$\left(H/M\right)^{1/\gamma} = a\left(T - T_C\right) + bM^{1/\beta} \qquad (9)$$

Where a and b are constants.

Figure 11 shows the arrott curves for several models $M^{1/\beta}$ vs $(H/M)^{1/\gamma}$: (a) Mean-Field model (β=0.5 and γ=1); (b) Tricritical mean-Field model (β=0.25 and γ=1) (c) 3D-Heisenberg model (β=0.365 and γ=1.336) and (d) 3D-Ising model (β=0.325 and γ=1.24).

Therefore, to select the model that best describes this system, it was calculated the Relative Slopes (RS) defined as [24]:

$$R_S = \frac{S(T)}{S(T_C)} \qquad (10)$$

Then, the proper model should be the one that has a value of R_S that is very close to unit. Figure 12 illustrates the relative slope as a function of temperature and demonstrates that the mean field model is best suited for our prepared.

The second order FM-PM transition is made evident by the modification of the Arrott curves (MAP) approach, which is based on the Arrott-Noakes formula [25] in determining the various critical exponents.

$$M_S = M_0(-\varepsilon)^{\beta}, \varepsilon < 0 \qquad (11)$$

$$\chi_0^{-1} = \left(h_0/M_0\right)(\varepsilon)^{\gamma}, \varepsilon > 0 \qquad (12)$$

$$M = DH^{1/\delta}, \varepsilon = 0 \qquad (13)$$

Where β, γ and δ are the critical parameters, M_0, h_0 and D, are the critical amplitudes, and $\varepsilon = (T-T_C)/T_C$ is the reduced temperature.

At high magnetic fields, the intersection of the axes of order and the axis of magnetization defines M_s (T) and χ_0^{-1}(T) in the Eq. 11 and the Eq. 12. M_S (T) and χ_0^{-1}(T) as a function of temperature have been illustrated in Figure 13.

The Kouvel Fisher method is an additional technique for determining the critical exponent β, γ and curie temperature T_C uses the following formula [26]:

$$\frac{M_s(T)}{\left(dM_s(T)/dT\right)} = \frac{T - T_C}{\beta} \qquad (14)$$

$$\frac{\chi_0^{-1}(T)}{\left(d\chi_0^{-1}(T)/dT\right)} = \frac{T - T_C}{\gamma} \qquad (15)$$

According to this method, the plotting of $M_S(T)[dM_S(T)/dT]^{-1}$ and $\chi_0^{-1}(T)[d\chi_0^{-1}(T)/dT]^{-1}$ against temperature, Figure 14, should yield straight lines with slopes of $\frac{1}{\beta}$ and $\frac{1}{\gamma}$, respectively, and the intercepts on the T axes are equal to T_C. The linear fitting to the plots following the KF method for our sample gives β for $T<T_C$ and γ for $T>T_C$. All critical exponent γ, β and T_C by the MAP and Kouvel Fisher method are summarized in Table 5. It is confirmed that the suitable is Mean-Field model with the MAP method and Kouvel Fisher method.

Conclusion

In this paper, the doping effect of 5 % of titanium on the compound $Pr_{0.9}Sr_{0.1}MnO_3$ elaborated by the solid-state method has been studied. The X-ray diffraction shows that the sample has an orthorhombic structure with a Pnma space group. The crystalline size D_{WH} exhibit an average size 28.24µm. The SEM micrographs reveal that the grains present an average size of 5µm. Magnetic analysis of our preparation $Pr_{0.9}Sr_{0.1}Mn_{0.95}Ti_{0.05}O_3$ indicates that the Curie temperature decreases compared to the parent sample, which is explained by the debility of the double exchange interaction. Magnetocaloric data shows that the sample has the potential to be a promising candidate for magnetic refrigeration. Critical behavior studies prove that MAP and Kouvel Fisher method adapts the Mean-Field model.

References

1. Ben Jazia Kharrat A, Boujelben W. Magnetic, Magnetocaloric and Correlation with Critical Behavior in Pr0.8Sr0.2MnO3 Compound Prepared via Solid-State Reaction. J Low Temp Phys. 2019; 197: 357-78.
2. Omrani H, Mansouri M, Cheikhrouhou Koubaa W, Koubaa M, Cheikhrouhou A. Critical behavior study near the paramagnetic to ferromagnetic phase transition temperature in $Pr_{0.6-x}Er_xCa_{0.1}Sr_{0.3}MnO_3$(x=0, 0.02 and 0.06) manganites. RSC Adv. 2016; 6: 78017-27.
3. Ah Dhahri E, Dhahri EK. Hlil. Phys A. 2014; 116: 2077-85.
4. Estemirova SKh, Mitrofanov VYa, Uporov SA, Gulyaeva RI. Effect of cation substitution on structural, magnetic and magnetocaloric properties of $(La_{0.7}Eu_{0.3})_{0.75}Sr_{0.25}Mn_{0.9}(Me)_{0.1}O_3$ (Me=Co, Ti). J Magn Magn Mater. 2020; 502: 166593.
5. Rostamnejadi A, Venkatesan M, Kameli P, Salamati H, Coey JMD. Magnetocaloric effect in $La_{0.67}Sr_{0.33}MnO_3$ manganite above room temperature. J Magn Magn Mater. 2011; 323: 2214-8.
6. Estemirova S, Mitrofanov V, Uporov S, Kozhina G. Structural and magnetic properties, magnetocaloric effect in $(La_{0.7}Pr_{0.3})_{0.8}Sr_{0.2}Mn_{0.9}Ti_{0.1}O_{3\pm\delta}$ (δ = 0.03, 0.02, −0.03). J Alloys Compd. 2018; 751: 96-106.
7. Rietveld HM. A profile refinement method for nuclear and magnetic structures. J Appl Crystallogr. 1969; 2: 65-71.
8. Roisnel T, Rodriguez-Carvajal J. Computer program FULLPROF, LLB-LCSIM; 2003.
9. Goldschmidt V. Die Gesetze der Krystallochemie. Naturwissenschaffen. Nat. 1926; 14: 1926 477.
10. Arayedh B, Kallel S, Kallel N, Peña O. Influence of non-magnetic and magnetic ions on the MagnetoCaloric properties of $La_{0.7}Sr_{0.3}Mn_{0.9}M_{0.1}O_3$ doped in the Mn sites by M=Cr, Sn, Ti. J Magn Magn Mater. 2014;361:68-73.
11. Khammassi F, Chérif W, Mendoza A, Jaramillo DS, Méndez SL, Dammak M. 2022; 128: 718.
12. Abdallah B. Master's degree. Tunisia: Faculty of Sciences of Sidi Bouzid; 2021.
13. Sekrafi HE, Ben Jazia Kharrat A, Chniba-Boudjada N, Boujelben W. Impact of B-site doping on magnetic and magnetocaloric effect of Pr0.75Bi0.05Sr0.1Ba0.1Mn1-xTixO3 (0≤x≤0.04) manganites. Solid State Sci. 2020; 105: 106274.
14. Dhahri I, Ellouze M, Mnasri T, Hlil EK, Jotania RB. J Mater Sci Mater Electron. 2020; 31: 12493-501.
15. Sekrafi HE, Ben Jazia Kharrat A, Chniba-Boudjada N, Boujelben W. Impact of B-site doping on magnetic and magnetocaloric effect of $Pr_{0.75}Bi_{0.05}Sr_{0.1}Ba_{0.1}Mn_{1-x}Ti_xO_3$ (0≤x≤0.04) manganites. Solid State Sci. 2020; 105: 106274.
16. Turki D, Cherif R, Hlil EK, Ellouze M, Elhalouani F. The effect of Co doping on structural, magnetic and magnetocaloric properties of $La_{0.8}Ca_{0.2}Mn_{1-x}Co_xO_3$ perovskites (0≤x≤0.3). Int J Mod Phys B. 2014; 28: 1450230.
17. Bouazizi A, Ellouze M, Labidi S, Hlil EK, Jotania RB. J Mater Sci Mater Electron. 2021; 32: 13089-99.
18. Cherif R, Hlil EK, Ellouze M, Elhalouani F, Obbade S. Magnetic and magnetocaloric properties of La0.6Pr0.1Sr0.3Mn1−xFexO3 (0≤x≤0.3) manganites. J Solid State Chem. 2014; 215: 271-6.
19. Bally MAA, Islam MA, Hoque SM, Rashid R, Fakhrul Islam Md, Khan FA. Magnetocaloric properties and analysis of the critical point exponents of $Pr_{0.55}Ca_xSr_{0.45-x}MnO_3$(x=0.00, 0.05, 0.1 and 0.2) at PM-FM phase transition. Results Phys. 2021; 28: 104546.
20. Mahjoub S, Baazaoui M, M'nassri R, Rahmouni H, Boudjada NC, et al. Effect of iron substitution on the structural, magnetic and magnetocaloric properties of $Pr_{0.6}Ca_{0.1}Sr_{0.3}Mn_{1-x}Fe_xO_3$(0⩽x⩽0.075) manganites. J Alloys Compd. 2014; 608: 191-6.
21. Raoufi T, Ehsani MH, Khoshnoud DS. Magnetocaloric properties of $La_{0.6}S_{r0.4}MnO_3$ prepared by solid state reaction method. J Alloys Compd. 2016; 689: 865-73.
22. Snini K, Ben Jemaa F, Ellouze M, Hlil EK. Structural, magnetic and magnetocaloric investigations in $Pr_{0.67}Ba_{0.22}Sr_{0.11}Mn_{1-x}Fe_xO_3$(0≤x≤0.15) manganite oxide. J Alloys Compd. 2018; 739: 948-54.
23. Elleuch F, Bekri M, Hussein M, Triki M, Dhahri E, et al. A-site-deficiency effect on critical behavior in the Pr0.6Sr0.4MnO3 compound. Dalton Trans. 2015; 44: 17712-9.
24. Ben Jemaa F, Mahmood SH, Ellouze M, Hlil EK, Halouani F. J Mater Sci Mater Electron. 2015; 26: 5381-92.
25. Saw AK, Hunagund S, Hadimani RL, Dayal V. Materials today. In: Proceedings of the https://www.sciencedirect.com/journal/materials-today-proceedings/vol/46/part/P14" \o "Go to table of contents for this volume/issue. 2021; 6218-22.
26. M'nassri R, Chniba-Boudjada N, Cheikhrouhou A. 3D-Ising ferromagnetic characteristics and magnetocaloric study in $Pr_{0.4}Eu_{0.2}Sr_{0.4}MnO_3$ manganite. J Alloys Compd. 2015; 640: 183-92.